NASA/TM–20210021872

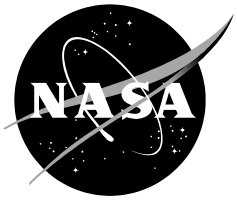

Vertical Climb Testing of the Model 699 Proprotor on the Tiltrotor Test Rig

C. W. Acree, Jr.
Ames Research Center
Moffett Field, California

December 2021

NASA STI Program Report Series

The NASA STI Program collects, organizes, provides for archiving, and disseminates NASA's STI. The NASA STI program provides access to the NTRS Registered and its public interface, the NASA Technical Reports Server, thus providing one of the largest collections of aeronautical and space science STI in the world. Results are published in both non-NASA channels and by NASA in the NASA STI Report Series, which includes the following report types:

- TECHNICAL PUBLICATION. Reports of completed research or a major significant phase of research that present the results of NASA Programs and include extensive data or theoretical analysis. Includes compilations of significant scientific and technical data and information deemed to be of continuing reference value. NASA counterpart of peer-reviewed formal professional papers but has less stringent limitations on manuscript length and extent of graphic presentations.

- TECHNICAL MEMORANDUM. Scientific and technical findings that are preliminary or of specialized interest, e.g., quick release reports, working papers, and bibliographies that contain minimal annotation. Does not contain extensive analysis.

- CONTRACTOR REPORT. Scientific and technical findings by NASA-sponsored contractors and grantees.

- CONFERENCE PUBLICATION. Collected papers from scientific and technical conferences, symposia, seminars, or other meetings sponsored or co-sponsored by NASA.

- SPECIAL PUBLICATION. Scientific, technical, or historical information from NASA programs, projects, and missions, often concerned with subjects having substantial public interest.

- TECHNICAL TRANSLATION. English-language translations of foreign scientific and technical material pertinent to NASA's mission.

Specialized services also include organizing and publishing research results, distributing specialized research announcements and feeds, providing information desk and personal search support, and enabling data exchange services.

For more information about the NASA STI program, see the following:

- Access the NASA STI program home page at http://www.sti.nasa.gov

- Help desk contact information:

https://www.sti.nasa.gov/sti-contact-form/
and select the "General" help request type.

NASA/ TM–20210021872

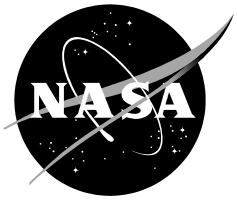

Vertical Climb Testing of the Model 699 Proprotor on the Tiltrotor Test Rig

C. W. Acree, Jr.
Ames Research Center
Moffett Field, California

National Aeronautics and
Space Administration

Ames Research Center
Moffett Field, California 94035-1000

December 2021

ACKNOWLEDGMENTS

The author wishes to thank Ethan Romander (NASA Ames Research Center) for his long-standing work to establish and maintain the PTR/JVX and TTR/699 databases, and Tom Norman (also NASA Ames) for his efforts to ensure data quality for the TTR/699.

Available from:

NASA STI Support Services
Mail Stop 148
NASA Langley Research Center
Hampton, VA 23681-2199
757-864-9658

National Technical Information Service
5301 Shawnee Road
Alexandria, VA 22312
webmail@ntis.gov
703-605-6000

This report is also available in electronic form at

http://ntrs.nasa.gov

TABLE OF CONTENTS

NOMENCLATURE

CFD	Computational Fluid Dynamics
HPP	Half Peak-to-Peak
JVX	Joint Vertical Experimental proprotor
NFAC	National Full-Scale Aerodynamics Complex
OARF	Outdoor Aerodynamic Research Facility
PTR	Prop Test Rig
TTR	Tiltrotor Test Rig
VS	Vane Set
40x80	40- by 80-ft NFAC test section
80x120	80- by 120-ft NFAC test section

A	Rotor disk area
c	Rotor chord (thrust weighted)
C_P	Power coefficient, $P/\rho A\, V_{tip}^3$
C_T	Thrust coefficient, $T/\rho A\, V_{tip}^2$
FM	Hover figure of merit, Tv_h/P
M_{tip}	Tip Mach number
N	Number of blades
P	Power
P_i	Rotor induced power
R	Rotor radius
T	Rotor thrust
v	Induced velocity
v_h	Induced velocity in hover, $\sqrt{T/2\rho A}$
V	Wind tunnel airspeed
V_{tip}	Rotor tip speed
η_c	Climb efficiency
ρ	Atmospheric density
σ	Rotor solidity, $Nc/\pi R$; or standard deviation

VERTICAL CLIMB TESTING OF THE MODEL 699 PROPROTOR ON THE TILTROTOR TEST RIG

C. W. Acree, Jr.

Ames Research Center

SUMMARY

The Tiltrotor Test Rig (TTR) is a new NASA asset for testing full-scale proprotors. The first test campaign in the National Full-Scale Aerodynamics Facility (NFAC) concluded in November 2018. The wind-tunnel test included vertical climb conditions simulated by axial flow at low airspeeds (true hover is not possible in the NFAC). The rotor tested was the Bell Model 699, an AW609 rotor modified specifically for wind-tunnel testing. The rotor was tested under a variety of NFAC configurations, some unprecedented and unique to vertical climb. This paper presents results for all test configurations applicable to vertical climb, including assessments of data quality. Comparisons with earlier tests of a similar rotor, the 0.656-scale Joint Vertical Experimental (JVX) rotor, are included to provide additional insights into rotor and wind tunnel behavior.

INTRODUCTION

The Tiltrotor Test Rig (TTR) is designed to test large-scale proprotors at high-speed axial flight up to 300 knots and tiltrotor conversion mode up to 180 knots. TTR can also test in helicopter mode up to 120 knots. The first entry of the TTR into the National Full-Scale Aerodynamics Complex (NFAC) was completed in November 2018. It was considered a checkout test focused on operational safety and efficiency, but the opportunity was used to collect rotor performance, loads, and acoustics data for research. The checkout test used the Bell Model 699 rotor (Fig. 1), which was built specifically for NASA by Bell and derived from the right-hand rotor of the Leonardo AW609.

Development of the TTR/699 is described in Ref. 1, and the test program is described in Refs. 2-4. References 5-7 document analytical studies of TTR/699 aeroelastic stability, performance, and airloads.

Low-speed vertical climb (near hover) is the focus of the present paper. The 699 rotor was tested under a variety of NFAC configurations, some unprecedented and unique to vertical climb. Researchers must understand the differences in configuration if they are to make proper use of the data. A similar rotor, the JVX (Joint Vertical Experimental) rotor, was earlier tested in both free air and in the NFAC. Data from those tests will be compared to the TTR/699 results. Far more data were acquired during the recent entry of the 699 rotor than during the JVX tests, so the former is necessarily given more emphasis.

NFAC tests where only the rotor is powered are frequently referred to as hover tests, simply because the drive fans are not used and airspeed is not controlled. For rotors installed with the shaft axis parallel to the flow direction (as shown in Fig. 1), the resulting test conditions are actually vertical climb with variable tunnel airspeed (rate of climb) because the rotor's induced velocity causes flow around the closed tunnel circuit.

Fig. 1. TTR/699 installed in the NFAC 40- by 80-ft test section, 0-deg yaw.

This paper first describes the TTR and 699 rotor, and summarizes key characteristics of the JVX rotor. The different test configurations of the NFAC used during the TTR and JVX entries are described. Examples of rotor performance data are presented, including checks of data repeatability. Selected loads, trim, and airspeed data are also presented to provide insight into wind-tunnel configuration effects on rotor behavior. The effects of rotor tip speed are also summarized. Many test conditions are the same as reported in Ref. 3, but all TTR/699 data were reprocessed for this paper, so the data points do not always match perfectly. This paper is a revision to an earlier paper, Ref. 8; key differences include thermally corrected rotor-balance data and aerodynamic tare corrections throughout.

A separate paper, Ref. 9 presents predictions of TTR/699 loads and performance, including extensive blade loads data. The present paper presents limited loads data for axial-flow conditions, but over a large variety of wind tunnel configurations.

TEST DESCRIPTION

TTR/699 and PTR/JVX Characteristics

The TTR is a horizontal axis rig, mounted in the NFAC 40- by 80-foot test section (Fig. 1). The TTR has sufficient power to drive the rotor to load limits in all flight conditions. Details of the TTR are summarized in Table 1.

The 699 rotor diameter is 26 ft and the geometric solidity is 0.097; thrust-weighted solidity is 0.0908. The rotor is stiff in-plane with a gimballed hub and yoke (flexbeam). The conversion and helicopter mode rotor speed is 569 rpm (M_{tip}=0.693) and the airplane mode (cruise) speed is 478 rpm (M_{tip}=0.580). Key characteristics are summarized in Table 2. Further details of the rotor design and test instrumentation may be found in Ref. 3.

Table 1. TTR Dimensions and Design Capabilities

Length, including spinner	435 in
Width, main nacelle only	85 in
Width, including pylons	140 in
Depth, main nacelle only	67 in
Weight, including rotor	60,800 lb
Rotor hub position:	
forward of balance center	88.5 in
height above floor (40x80)	234 in
Power, max design	6,000 hp
Power, max (30 min)	5,500 hp
Power, continuous (2 hr)	5,000 hp
Rotor shaft speed, max	629.5 rpm
Max airspeed, 0 deg yaw	300 knots (305 lb/ft^2)*
Max airspeed, 90 deg yaw	180 knots (110 lb/ft^2)*

*40x80 limit=262 lb/ft^2, 80x120 limit=33 lb/ft^2

Table 2. TTR/699 Rotor Characteristics

Number of blades	3
Diameter	26.0 ft
Disc area (per rotor)	530.9 ft^2
Solidity (thrust weighted)	0.0908
Blade chord (thrust weighted)	14.83 in
Blade area (per rotor)	48.2 ft^2
Blade twist (non-linear)	−47.5 deg
Blade taper ratio (linear)	0.684
Blade tip shape	square
100% rotor speed (helicopter mode)	569 rpm
Tip speed	775 ft/sec
84% rotor speed (airplane mode)	478 rpm
Tip speed	651 ft/sec
Gimbal limit (flapping stop)	±11 deg
Precone	2.75 deg
Undersling	0.36 in
Delta-3, maximum (pitch horns level)	−15 deg
Direction of rotation (looking aft)*	CCW

*As installed on TTR.

Although built in the same blade molds as the production AW609 rotor, the Bell 699 rotor is unique: the 699 has no deicing or pendulum absorbers, and has special instrumentation and modified controls as appropriate for a wind-tunnel test article. The pitch horn lugs are inverted to connect to the TTR control system.

TTR Rotor Balance

The TTR rotor loads measurement system, commonly referred to as the "rotor balance," was calibrated when installed on the TTR. Calibration procedures are described in Refs. 1 and 10; the results are summarized in Table 3. For the record, the rotor balance data reported here use the "B3" balance calibration and include time-interpolated corrections for zero offsets. The wind-tunnel scales were locked, so all rotor loads were measured by the balance.

The TTR rotor balance is overdesigned for the 699 rotor. The rotor has a gimballed hub, so it cannot sustain large moments. The 699 rotor has a maximum thrust just over 1/2 of the balance range, maximum hub moments 1/8 of the balance range, and maximum torque less than 1/3 of the torque tube range. The balance was calibrated over different load ranges (Ref. 1); Table 3 gives calibration uncertainties referenced to the reduced load ranges appropriate for the 699 rotor.

Table 3. TTR Rotor Balance Calibration

Hub Load	Calibration Range	2σ / Range
Normal force (thrust)	15,148 lb	0.80 %
In-plane horizontal	±8,250 lb	0.15 %
In-plane vertical	±8,250 lb	0.11 %
Hub moment, vertical axis	±7,500 ft-lb	1.16 %
Hub moment, horizontal	±7,500 ft-lb	1.50 %
Torque	22,338 ft-lb	0.42 %

JVX vs 699 Rotors

The JVX rotor was tested on the Prop Test Rig (PTR) in free air at the Outdoor Aerodynamic Research Facility (OARF) and in the NFAC. The PTR had half the power and thrust capability of the TTR. See Refs. 11 and 12 for details of the JVX rotor and PTR; Ref. 11 discusses the PTR rotor balance.

Table 4 summarizes major differences between the 699 and JVX rotors. The latter is sometimes referred to as a "2/3-scale V-22", and more rarely as the "M901" rotor; the scale is in fact 0.656 relative to V-22. The 699 rotor uses a gimballed hub with a coning flexure similar to the V-22, whereas the JVX rotor was tested with an XV-15 hub with fixed precone. Both rotors have a small amount of structural sweep, with the quarter-chord line intersecting the pitch axis at 75% radius. The values in Table 4 are equivalent aerodynamic sweep. The V-22 rotor has a blade-fold hinge covered by a large cuff, and the JVX rotor had a similar cuff to simulate the V-22. The 699 has no folding hinge, hence no cuff; its blade is tapered at the root for a clean intersection with the spinner.

For both the PTR and TTR, the rotor controls are inside the spinner. The layout of the control system has no effect on aerodynamics, but the geometry does affect pitch-link loads. The TTR has a conventional swashplate with pitch links connecting to the pitch horns from aft of (below) the rotor. The JVX pitch links are connected to overhead walking beams. Consequently, the magnitudes of the pitch link loads are slightly different and the polarity is reversed, even for identical blade loads.

Table 4. Key Differences Between 699 and JVX Rotors

Feature	699	JVX
Diameter	26 ft	25 ft
Solidity	0.0908	0.1138
Taper	0.684	0.646
Precone	2.75 deg, flexure	2.5 deg, fixed
Sweep	1.45 deg	1.91 deg
Hover tip speed	775 ft/sec	790 ft/sec
Root	Tapered	Cuffed
Controls	Conventional	Overhead

NFAC Test Configurations

Rotor tests in the NFAC are not capable of true hover, at least not at the scale of the 699 rotor. There is always duct flow due to the test section walls, even with the drive fans inactive. Depending on configuration, some amount of flow circulates around the entire wind tunnel. Thus, TTR tests without the drive fans simulate vertical climb.

The cross-section of the 40x80 test section used for the TTR/699 test is a flattened oval (Fig. 1), with a square center flanked by two semi-circles. The literal dimensions are 39 by 79 ft (an acoustic lining slightly reduces the usable area). The NFAC flow circuit can be configured in different ways, normally as a closed-circuit tunnel at high speeds, or as an open circuit at low speeds. For the TTR, however, several unorthodox configurations were tested to determine their effects on rotor performance and loads.

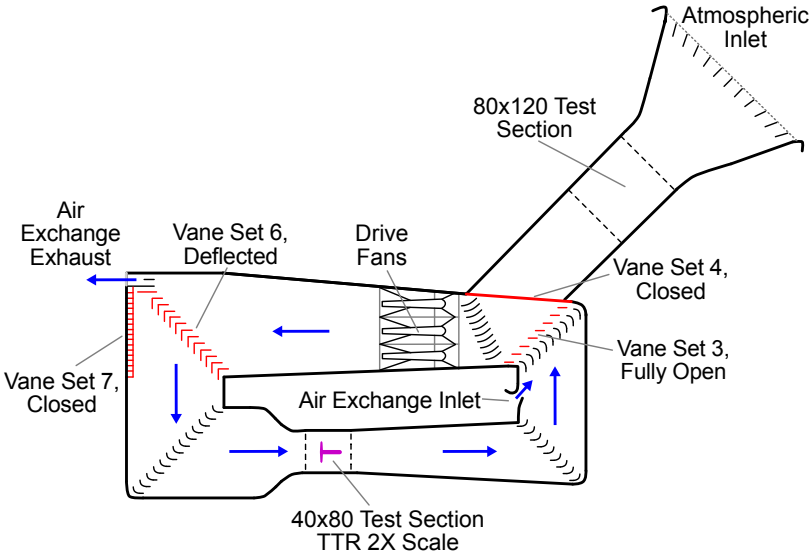

Fig. 2. The NFAC configured for normal 40x80 operations, with the TTR at 0-deg yaw angle (config. A).

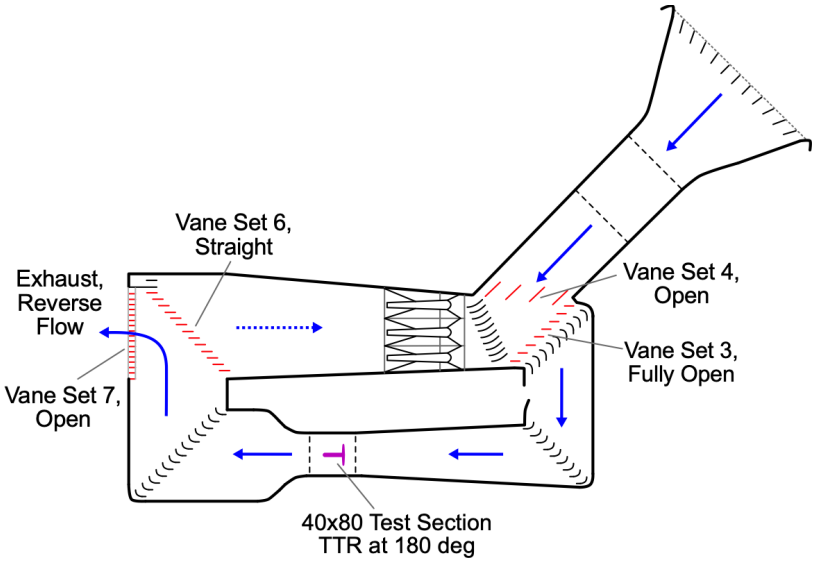

Fig. 3. The NFAC configured for reverse-flow operations, with the TTR at 180-deg yaw angle (config. B2).

Figures 2 and 3 show two different NFAC configurations, with the differences highlighted. All TTR/699 data were taken with some combination of the settings shown in Figs. 2 and 3, as listed in Table 5. Not all combinations are mechanically possible. In particular, Vane Set 6 (VS 6) is always matched to VS 7: if VS 7 is closed, VS 6 is set to turn the flow (Fig. 2), but if VS 7 is open, VS 6 is straight (Fig. 3). Several possible combinations were omitted because of poor initial results or high loads, notably with the TTR at 180-deg yaw.

Table 5 lists the seven configurations of the NFAC used to determine facility effects on TTR/699 rotor behavior. Research data were taken over twelve runs. The notation used in Table 5 for the Vane Set configuration is unique to this paper. Vane Set 3 has eight panels; only four or two of the inboard panels were open for configurations D2 and D3, respectively. An eighth configuration, with the overhead doors open, was used exclusively for the PTR/JVX.

The rotor is pointing in the upstream direction at 0-deg yaw (Figs. 1 and 2), and in the reverse direction at 180-deg yaw (Fig. 3). Most data were taken at M_{tip}=0.693 (569 rpm). Runs 102 and 110 included data at both M_{tip}=0.693 and M_{tip}= 0.583 (479 rpm). Run 78 was a motor test at fixed shaft speed (478 rpm), so M_{tip} does not match perfectly with Runs 102 and 110.

Run 60 was slightly limited in thrust because of conservative hub-load limits. After a review of the data, the limits were raised for Run 61. Maximum TTR/699 thrust was always limited by hub loads, not blade loads or power. Higher load limits are not necessarily of value in flight: at thrust higher than needed to trim at gross weight, the aircraft will either accelerate or climb, thereby changing the flow conditions. Maximum achieved thrust is in some respects a result of ground testing and not a fundamental limitation of the rotor.

Table 5. NFAC Configurations for TTR/699 Hover/Vertical Climb

Config.	Run	Yaw	VS 3	VS 4	VS 6/7	Notes
A	59	0	open	closed	closed	limited data
A	60	0	open	closed	closed	
A	61	0	open	closed	closed	higher load limits
A	78	0	open	closed	closed	motor test, fixed rpm
B1	62	180	open	closed	closed	
B2	63	180	open	closed	open	
C	99	0	open	closed	open	motor test, limited data
C	100	0	open	closed	open	motor test, limited data
C	110	0	open	closed	open	2 tip speeds
D1	101	0	open	open	open	
D2	102	0	4/8 open	open	open	2 tip speeds
D3	103	0	2/8 open	open	open	
E	JVX	180	1/8 open	open	open	overhead doors open

For completeness, the table includes a few runs that yielded only limited research data. Run 59 was a procedural checkout run (the last track and balance run). Runs 99 and 100 were motor tests with very few data points. Those three runs are not analyzed in detail.

The standard NFAC configuration for closed-circuit operations is shown in Fig. 2. Vane Sets 4 and 7 are closed, forcing the air to complete the circuit, as required for high-speed operations with the 40- by 80-foot test section (40x80 mode).

Normally, use of the 80- by 120-foot test section (80x120 mode) requires Vane Sets 4 and 7 to be open, and Vane Set 3 closed, effectively blocking flow through the 40x80 test section. A variant of this configuration was used for several runs, with Vane Set 3 fully or partially open to allow flow through the 40x80 test section while minimizing flow around the entire circuit (Fig. 3). This configuration is inefficient, but allows the TTR to be oriented in the reverse direction. For testing rotors in low-speed vertical climb, the inefficiency is beneficial because the free-stream velocity is reduced.

The 1988 test of the JVX rotor used a unique NFAC configuration, with the rotor at 180-deg yaw, Vane Set 7 (the main exhaust) open, Vane Set 3 closed (all but one panel), and the test-section overhead doors open (Ref. 13). The overhead opening spanned 49 by 78.5 feet: a larger area than the 40x80 cross section. Safety requirements precluded use of this configuration for TTR testing.

HISTORY: PTR/JVX TESTS

Figure 4 shows the PTR/JVX as tested at the OARF in 1984 (Ref. 11). Figure 5 shows the PTR/JVX in the NFAC 40x80 test section at 0 deg yaw (Refs. 13 and 14). Figure 5 also shows part of the opened overhead doors; the opened personnel access door is partially hidden behind the support pylon at the lower left.

Fig. 4. Scaled JVX rotor on the Prop Test Rig at the OARF (1984).

Fig. 5. Scaled JVX rotor on the Prop Test Rig in the NFAC (1991).

Figure 6 plots figure of merit versus thrust for the OARF and 40x80 JVX tests. Very limited data were taken at equal tip speeds; the two speeds shown are the closest for which good thrust sweeps are available. The 40x80 data shown here were taken at 180 deg yaw (the reverse of Fig. 5). For the OARF test, C_P was corrected for wind per Ref. 11; the wind-tunnel data had no airspeed corrections.

The near match of the two JVX data sets from the OARF and NFAC tests gave hope that the 40x80 test section could be used to accurately simulate hover. The JVX and 699 rotors are closely similar, so comparing results for the two rotors would provide traceability from hover through vertical climb and ultimately high-speed airplane mode (Ref. 3).

However, the apparently good results of Fig. 6 are misleading. Figure 7 plots airspeed for the two tests. For the OARF data, airspeed is wind speed from any direction, whereas the 40x80 data is airspeed in the test section as generated by the rotor. Momentum theory suggests that figure of merit should *not* match, given the different airspeeds.

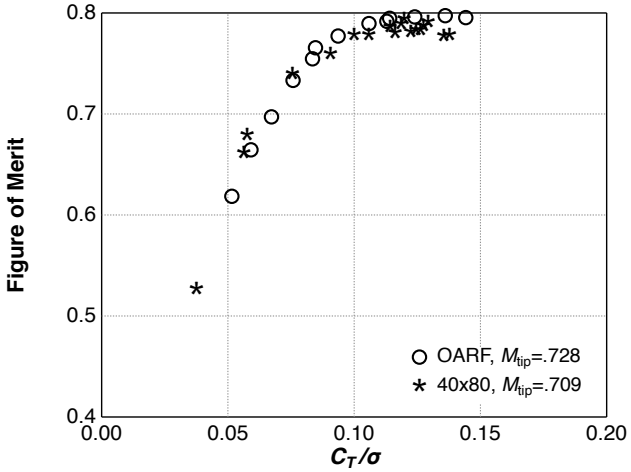

Fig. 6. JVX figure of merit, OARF vs. 40x80 tests.

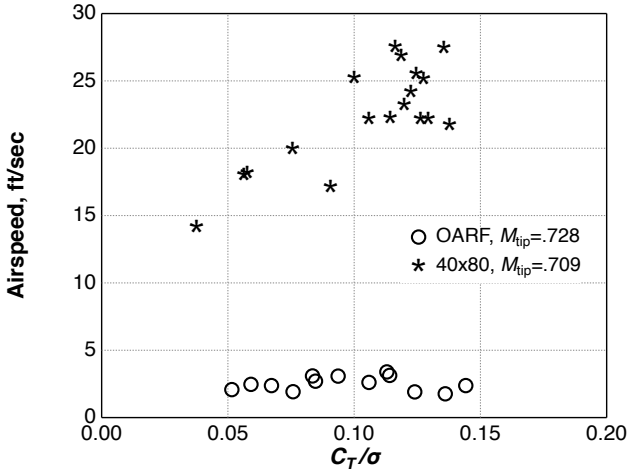

Fig. 7. JVX airspeed, OARF vs. 40x80 tests.

Reference 15 gives the classic momentum-theory solution for minimum possible power for a rotor in axial flow:

$$P_i = T(V + v) = T\left(V/2 + \sqrt{(V/2)^2 + {v_h}^2}\right) \quad (1)$$

$$v_h = \sqrt{T/2\rho A} \quad (2)$$

where P_i = ideal power, T = thrust, V = airspeed, A = rotor disk area, ρ = density, v = induced velocity, and v_h = induced velocity in hover. In this paper, V is always the net wind-tunnel velocity generated by the rotor. Airspeed is here defined with respect to the rotor, so the airspeed is always positive.

In contrast, rotor figure of merit is traditionally defined as:

$$FM = Tv_h/P = T\sqrt{T/2\rho A}/P \quad (3)$$

where P is measured power.

Figure 8 plots the ratio of ideal power in climb (V >0) to ideal power in hover (V=0) as a function of thrust for several different airspeeds (rates of climb). At the airspeeds measured during the hover and climb runs, the difference in ideal power is roughly 25%, which should result in a distinct difference in efficiency relative to figure of merit. A more appropriate efficiency metric is suggested in the next section.

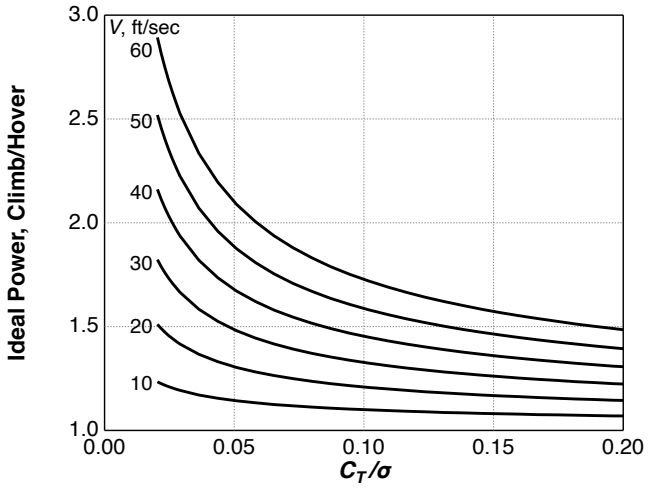

Fig. 8. JVX hover/climb ideal power ratio; V_{tip}=775 ft/sec.

VERTICAL CLIMB RESULTS

In the NFAC 40x80 test section, true hover (wind off) is impossible for large rotors because the effects of the tunnel walls cannot be avoided. Furthermore, the rotor's induced velocity continues around the tunnel circuit without completely dissipating, so the test conditions are actually low-speed vertical climb. The PTR/JVX test attempted to mitigate this effect by opening the overhead doors, with mixed results as will be shown.

In the wind tunnel, the rotor is trimmed to M_{tip} not rpm, so the actual tip speed varies with wind tunnel temperature. Following standard NFAC practice, the TTR/699 rotor was trimmed to zero flapping for all performance data points. However, zero flapping was not as precisely achieved during the JVX test.

Figure 9 plots figure of merit for the TTR/699 thrust sweeps in Table 5 at nominal hover M_{tip}=0.684. Runs 59, 78, and 100 are excluded because they produced limited data or were not rigorously trimmed to constant tip speed. Figure 10 plots airspeed for the same data points as Fig. 9. The airspeed trends are slightly more evident when plotted against physical thrust, as in Fig. 10. JVX data for the 40x80 test are also included; those data were taken at M_{tip}=0.709 and are the same as plotted in Figs. 6 and 7. Both figure of merit and airspeed show a strong dependency on wind-tunnel configuration. Data at airplane-mode tip speed are given in a later section. Separation of figure of merit into distinct bands, generally correlated with airspeed, is evident in Figs. 9 and 10.

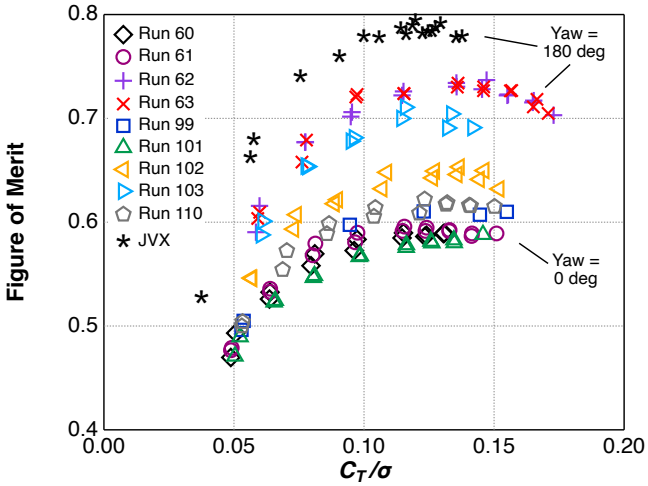

Fig. 9. TTR/699 figure of merit vs. thrust at M_{tip}=0.684; PTR/JVX data at M_{tip}=0.709.

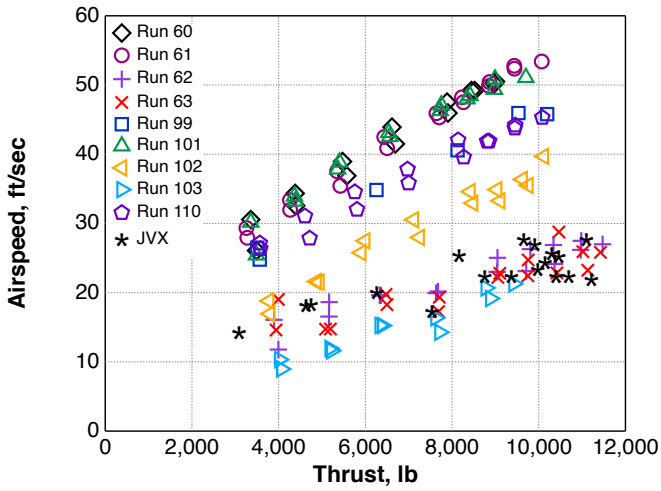

Fig. 10. TTR/699 airspeed vs. thrust at M_{tip}=0.684; PTR/JVX data at M_{tip}=0.709.

Climb Efficiency Metric

Neither figure of merit nor propulsive efficiency are strictly appropriate for the operating conditions discussed here. Given non-zero airspeed, figure of merit is not a true measure of efficiency but remains a useful way of plotting power.

We can define climb efficiency $\eta_c = P_i/P$, where P_i is defined in Eqn. 1 and P is measured power. As $V \rightarrow 0$, η_c becomes rotor figure of merit, and for $V >> v$, η_c approaches propeller propulsive efficiency $\eta = TV/P$.

Earlier papers (Refs. 3 and 12) applied the Glauert velocity correction (Ref. 16) to account for the influence of the tunnel walls. However, the Glauert velocity correction is problematic for JVX hover/climb data in the 40x80 because the large opening at the top of the test section violates the assumptions of Glauert's analysis. The uncorrected climb efficiency is less representative of flight but is more consistent between PTR/JVX and TTR/699 tests and is therefore more appropriate for comparing data taken in the NFAC.

There remains the problem of measuring airspeed with the rotor at 180-deg yaw. The NFAC air data system uses two sets of pressure transducers upstream of the test section to measure velocity, where upstream is defined for normal 40x80 operations (Fig. 2 and Table 5 configuration A). The system is not calibrated for reverse flow with the PTR or TTR installed, nor are the measurements corrected for the additional velocity induced by the rotor. The net effects of induced velocity, nacelle and strut drag, blockage, and wake turbulence are unknown, as are the effects of the open overhead doors during the JVX test. Experimental investigation of such effects would be welcome but was far beyond the scope of the TTR checkout test. CFD studies have been initiated in hopes of gaining insight into the likely magnitude of needed corrections. For the present paper, the standard NFAC velocity measurements are used without correction for 180-deg yaw for both PTR/JVX and TTR/699 data.

Figure 11 plots climb efficiency η_c for the same conditions as Figs. 9 and 10. The results are far more consistent than figure of merit, with Run 103 and the JVX data clear outliers. Run 103 (configuration D3) had the most restrictive setting on Vane Set 3 of all 699 data. The JVX data had an even more restrictive setting on Vane Set 3 (Table 5).

The 699 achieved higher thrust at 180-deg yaw than at 0-deg yaw. While the JVX data achieved higher figure of merit and climb efficiency than the 699, the scatter in η_c is much worse than any 699 test configuration (Fig. 11a). Restricting Vane Set 3 beyond half open (4/8, Table 5) increased figure of merit (Run 103 and JVX, Fig. 9) but had the opposite effect on η_c (Fig. 11). However, the JVX data also had the overhead doors open. The effects on loads and trim are examined further below.

Figure 11(a) is very cluttered, so Fig. 11(b) presents a reduced data set comprising only 699 data at 0-deg yaw and M_{tip}=0.684. Run 60 data are omitted because they are redundant to Run 61. More detailed comparisons of different yaw angles and tip speeds are presented in the following sections.

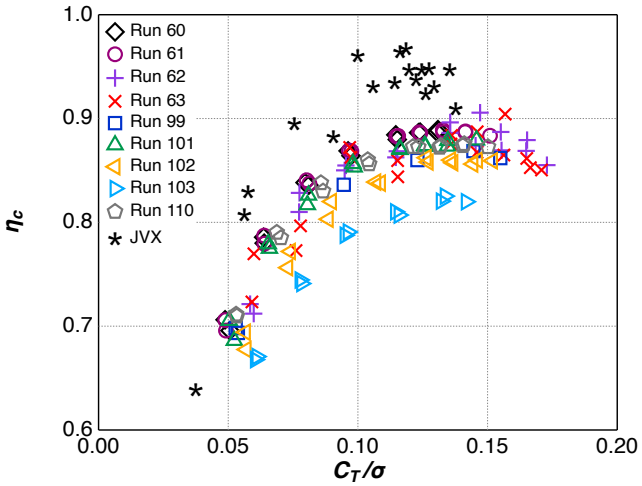

(a) TTR/699 data at M_{tip}=0.684; PTR/JVX data at M_{tip}=0.709.

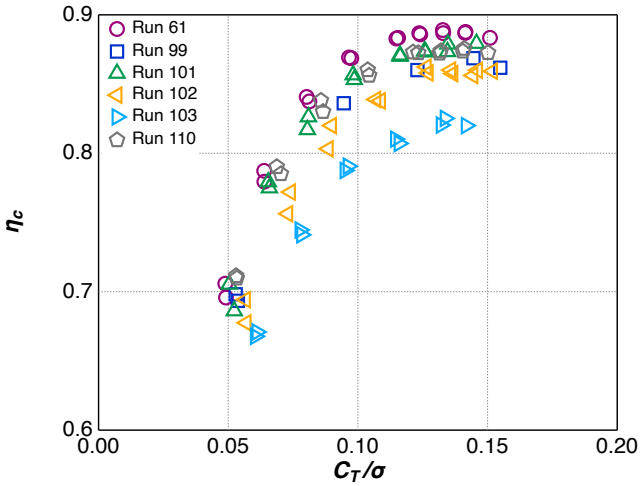

(b) TTR/699 climb efficiency vs. thrust at 0-deg yaw, M_{tip}=0.684.

Fig. 11. Climb efficiency vs. thrust at helicopter-mode tip speed.

Loads and Trim

A comprehensive survey of loads would normally include both blade and hub loads (see Ref. 11 for a survey of the TTR/699 test data). The limiting loads during the 699 runs shown here (Table 5) were almost always hub loads. The scaled JVX rotor used a completely different hub design than the 699 rotor, so direct comparisons of internal hub loads would be misleading. Fortunately, 699 unsteady pitch-link loads generally tracked hub loads, so the former can be used as a common reference between the 699 and JVX rotors. The TTR and PTR used different control systems and the two rotors have different solidity, so unsteady pitch-link loads were divided by the absolute value of mean loads to cancel out the effects of geometry. All 699 pitch-link data shown here are for the "white" blade.

Unsteady thrust loads, as measured by the rotor balance, are also useful for evaluating the effects of wind-tunnel configuration. Unfortunately, no unsteady thrust loads are available for the JVX rotor.

Figure 12 plots one-half peak-to-peak (HPP) thrust versus steady thrust. Again, Run 103 is an outlier. Runs 62 and 63—the two runs at 180 deg—also have higher unsteady loads than the other data. Runs 60 and 61—the runs in the standard 40x80 configuration—have the lowest unsteady loads. Pitch-link loads show similar results. Pitch-link loads are plotted in two ways: normalized in Fig. 13(a) and in physical units in Fig. 13(b). Pitch-link loads in physical units are higher for JVX than for 699, as would be expected for a rotor with 25% higher solidity, but the 699 rotor achieved higher maximum thrust despite its lower solidity.

The high unsteady loads seen at 180-deg yaw were the reason that configuration was not explored as thoroughly as 0-deg yaw. Run 62, with Vane Sets 4 and 6/7 closed, had slightly higher loads than Run 63 with all Vane Sets open. Run 103, 0-deg yaw with Vane Set 3 mostly closed, also had very high loads.

Allowing the air to circulate backwards around the wind tunnel caused much higher unsteady loads than forward flow (configurations B1 and B2 vs. A). While this result is not surprising—the NFAC is not designed for reverse flow—the magnitude of the effect at low airspeed was unexpected. At 180-deg yaw, opening the exhaust (configuration B1 vs. B2) had negligible effect on airspeed and a minor effect on unsteady loads; compare Runs 62 and 63.

At 0-deg yaw, restricting the flow by closing Vane Set 3 (configurations D1, D2, and D3) progressively reduced airspeed, which also reduced η_c; compare Runs 101, 102, and 103, Fig. 10. However, closing Vane Set 3 did not result in higher achievable thrust, and caused much higher unsteady loads at maximum restriction (configuration D3, Run 103).

The preceding figures are densely plotted, so significant data (699 Runs 61-63 and JVX) are replotted in Figs. 14-16. Figure 17 adds longitudinal gimbal angle. TTR/699 Run 60 is omitted because its maximum thrust was restricted. Figures 19 and 20 plot the same data as Figs. 16 and 17, but against airspeed instead of thrust. Surviving JVX loads data are incomplete, so a few data points are missing.

These figures emphasize that the 180-deg yaw configurations yielded higher thrust than the 0-deg yaw configurations, but also higher unsteady loads. For the 699, no configuration had lower unsteady loads than the standard 40x80 configuration (Runs 60 and 61). No 0-deg yaw configuration achieved thrust as high as either 180-deg yaw configuration (runs 62 and 63). The JVX data had far more scatter and higher unsteady loads than the 699 data taken at favorable configurations (A, C, D1, and D2).

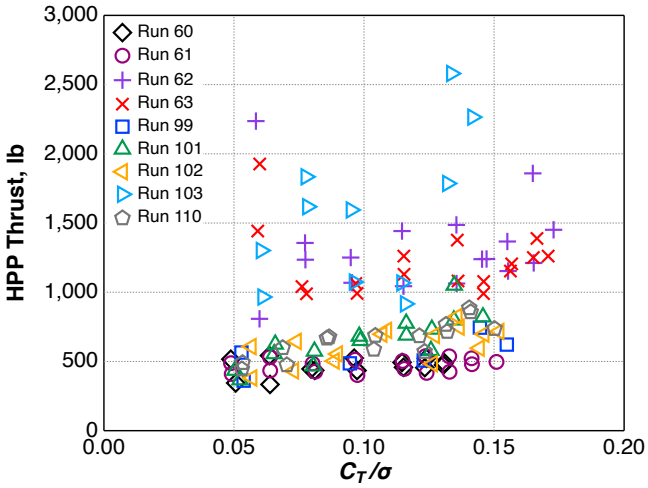

Fig. 12. TTR/699 unsteady thrust vs. steady thrust at M_{tip}=0.684.

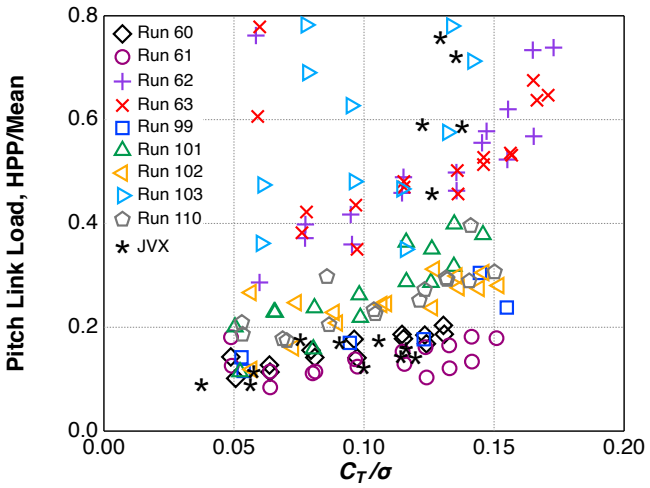

(a) Unsteady pitch-link loads, normalized against mean loads.

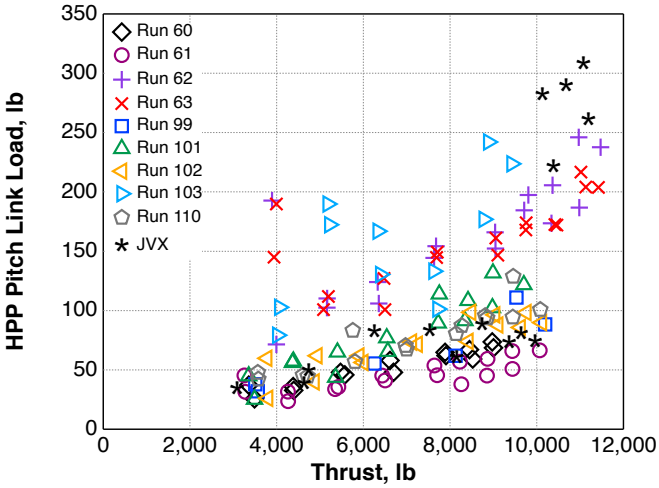

(b) Unsteady pitch-link loads, in physical units.

Fig. 13. TTR/699 unsteady pitch-link loads vs. thrust at M_{tip}=0.684; PTR/JVX data at M_{tip}=0.709.

Furthermore, the JVX was not trimmed as well as the 699 at high thrust (Fig. 17). The largest longitudinal gimbal angle may be small at just over 1 deg at C_T/σ = 0.137 (11,200 lb), but at that thrust the gimbal angle generates over 200 lb of untrimmed in-plane load. The JVX longitudinal gimbal angle varies considerably and nonlinearly with thrust (Fig. 17) and varies inconsistently with airspeed (Fig. 20); the rotor is obviously not trimmed to zero flapping. This effect was likely caused by the asymmetric flow generated by the open overhead doors.

In contrast, the maximum lateral gimbal angle was always less than ±0.2 deg for both rotors (not shown). Moreover, the TTR/699 longitudinal gimbal angle was within ±0.2 deg for all but the first two data points from Runs 62 and 63, at lowest thrust (Fig. 17).

Figure 18 emphasizes that both the PTR/JVX and TTR/699 generated similar wind-tunnel airspeeds at 180-deg yaw. Opening the overhead doors did not appreciably reduce airspeed, but in some cases led to pitch-link loads as high as the 699 data with the highest loads at the same airspeed (Fig. 19). The large scatter and inconsistent trends in JVX gimbal angle and pitch-link load are unexplained.

Runs 61 and 62 both had the vane sets in the same configuration, so the only difference was the rotor orientation. The wind-tunnel velocity induced by the rotor is higher at 0-deg yaw (Run 61) than at 180-deg yaw (Fig. 18), so the rotor is operating a higher effective rate of climb.

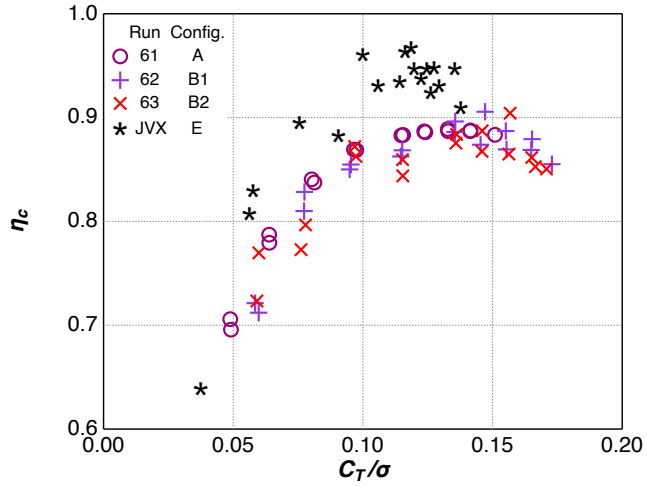

Fig. 14. Climb efficiency vs. thrust for selected data.

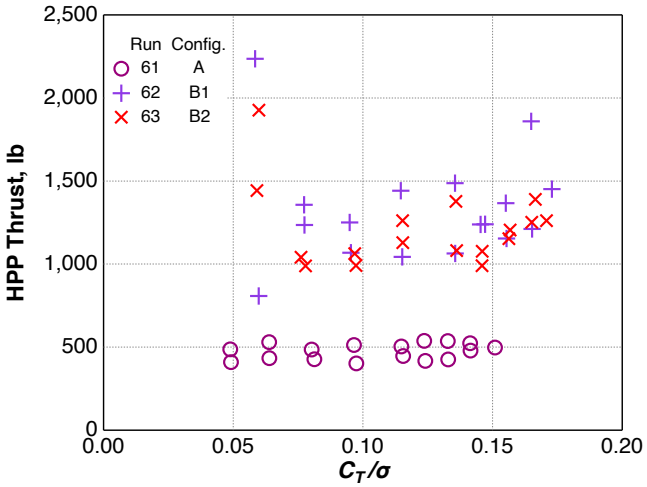

Fig. 15. Unsteady thrust vs. steady thrust for selected data.

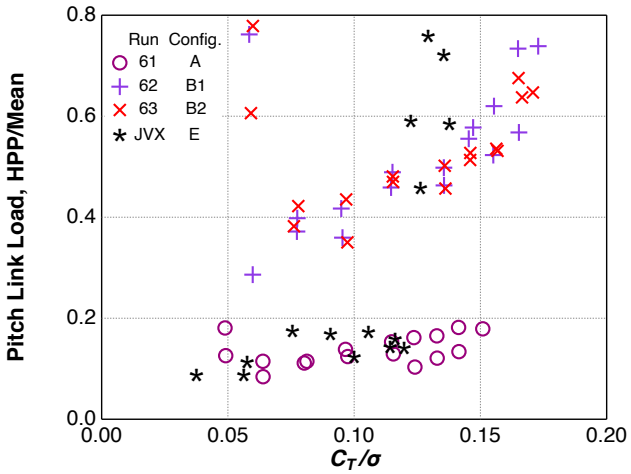

Fig. 16. Unsteady pitch-link loads vs. thrust for selected data**.**

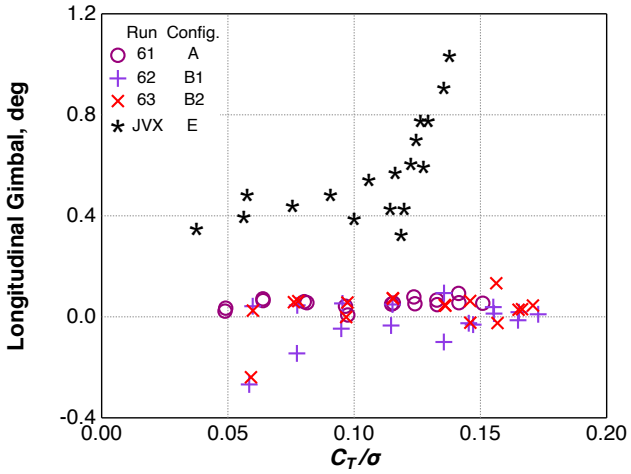

Fig. 17. Trimmed gimbal angle vs. thrust for selected data.

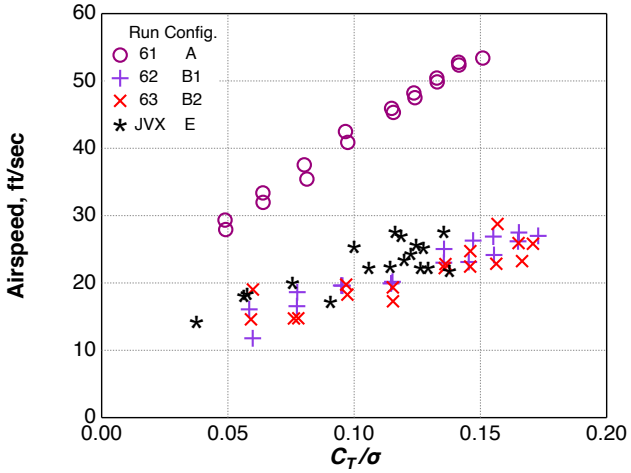

Fig. 18. Airspeed vs. thrust for selected data.

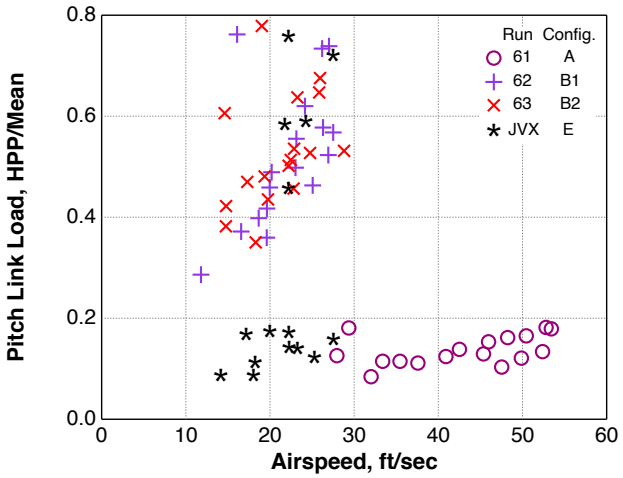

Fig. 19. Unsteady pitch-link loads vs. airspeed for selected data.

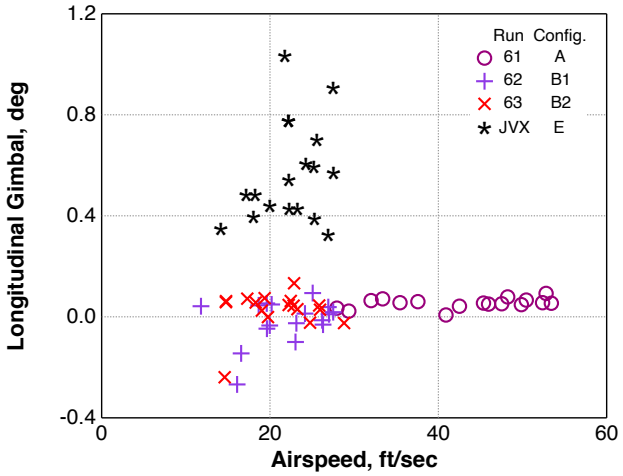

Fig. 20. Trimmed gimbal angle vs. airspeed for selected data.

Tip Speed Comparisons

Reduced Tip Speed, M_{tip}=0.583

Three thrust sweeps were performed for the 699 at airplane-mode tip speed, M_{tip}=0.583 (84% of helicopter mode). Run 78 was a motor test at fixed rpm, not tip Mach number, so its tip speed was slightly low at M_{tip}=0.580. The reduced-rpm runs were performed as the opportunity arose, so each had a different vane set configuration with little attempt at systematic variation. Figures 21-25 summarize the results. Filled symbols denote data taken at airplane-mode tip speed.

At the lower tip speed, the data fall into distinct bands for both figure of merit and climb efficiency (Figs. 21 and 23). The lower the airspeed, the higher the figure of merit and the lower the climb efficiency, most evidently for Run 102. As seen at the higher tip speed, configuration A had the lowest unsteady loads (Figs. 24 and 25). The effects of tip speed at a given configuration are explored in more detail in the following section.

Limited JVX data were taken at reduced tip speed. C_T/σ =0.1 was the maximum thrust achieved, which is not enough for a useful comparison. The JVX data are therefore omitted from Figs. 21-25.

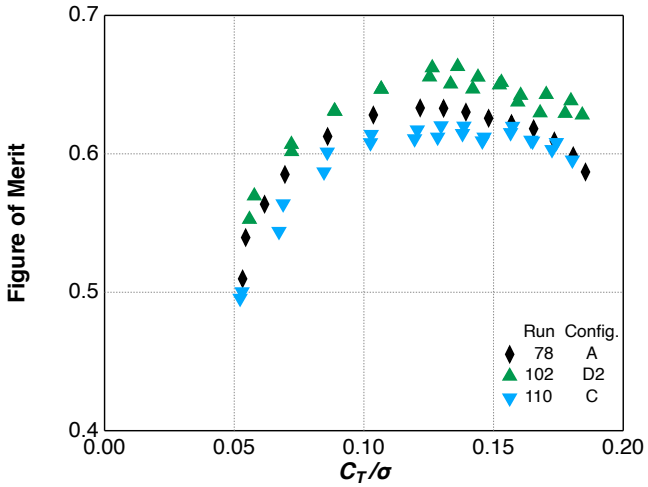

Fig. 21. TTR/699 figure of merit vs. thrust at M_{tip}=0.583.

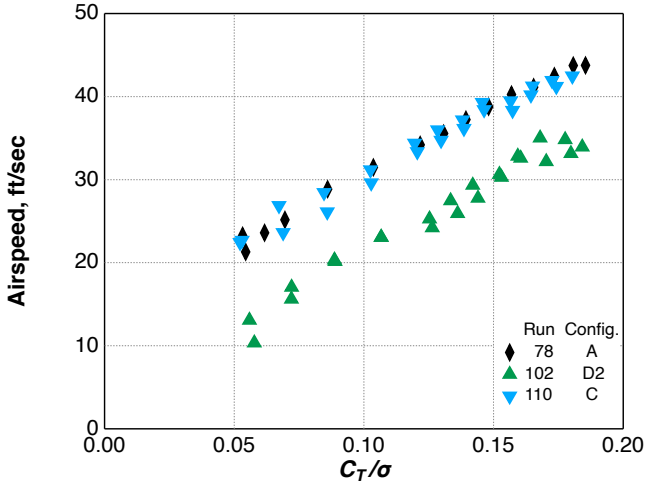

Fig. 22. TTR/699 airspeed vs. thrust at M_{tip}=0.583.

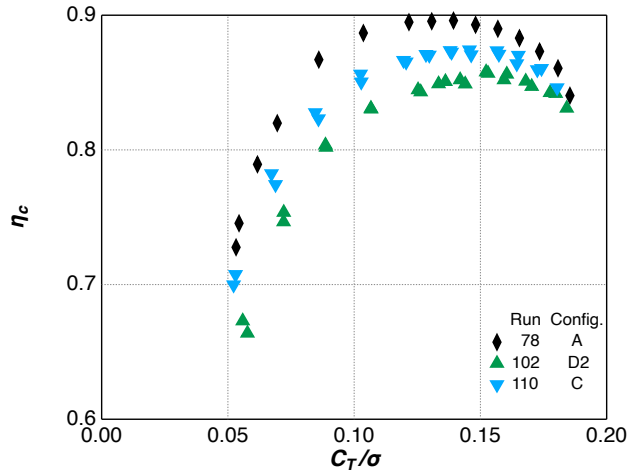

Fig. 23. TTR/699 climb efficiency vs. thrust at M_{tip}=0.583.

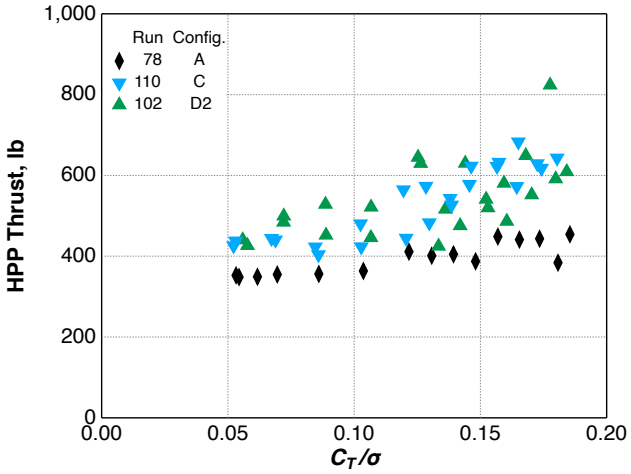

Fig. 24. TTR/699 unsteady thrust vs. steady thrust at M_{tip}=0.583.

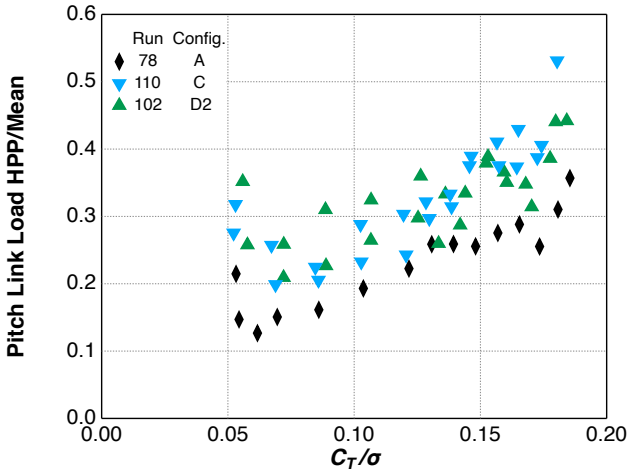

Fig. 25. TTR/699 unsteady pitch-link loads vs. thrust at M_{tip}=0.583.

Effects of Tip Speed

For three configurations (A, D2, and C), the 699 rotor was operated at two different tip Mach numbers. Figures 26-29 replot the data already presented for Runs 61, 78, 102 and 110 to highlight the differences. Open and filled symbols respectively denote helicopter- and airplane-mode tip speed. Airspeed is again plotted against physical thrust, which clearly shows the data separation into distinct bands. For Runs 102 and 110, (configurations D2 and C), the thrust sweeps for the two tip speeds were run back-to-back. For configuration A, however, Runs 61 and 78 were run several weeks apart, when the ambient temperature was different. For the nondimensional coefficient η_c, the data for each configuration follow consistent trends (Fig. 26). In contrast, the effect of temperature on airspeed is evident when plotted in physical units (Fig. 27).

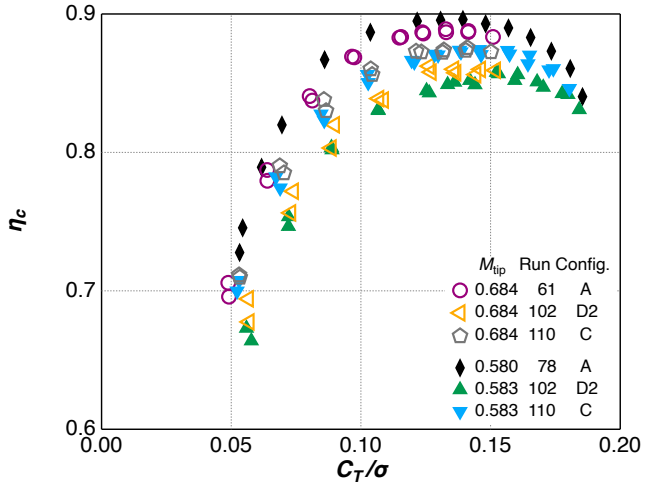

Fig. 26. TTR/699 climb efficiency vs. thrust at two tip speeds.

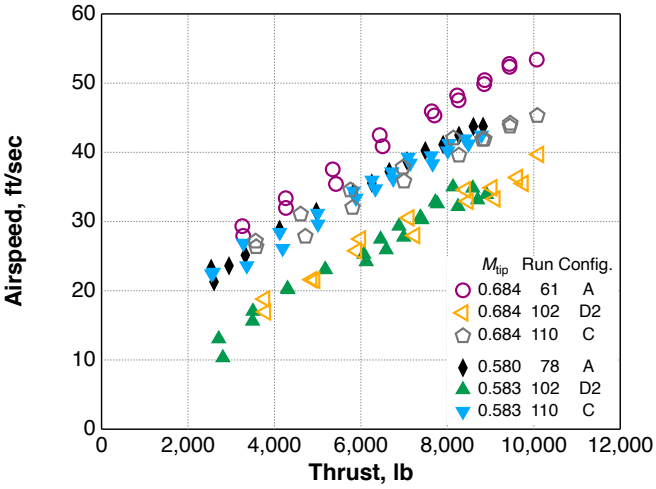

Fig. 27. TTR/699 airspeed vs. thrust (lb) at two tip speeds.

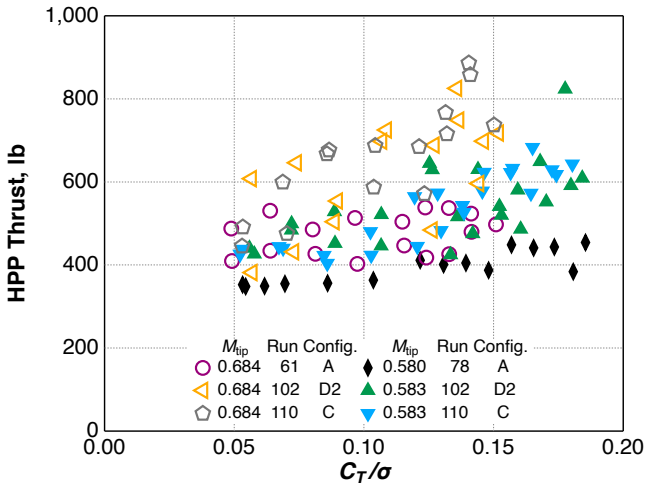

Fig. 28. TTR/699 unsteady thrust vs. steady thrust at two tip speeds**.**

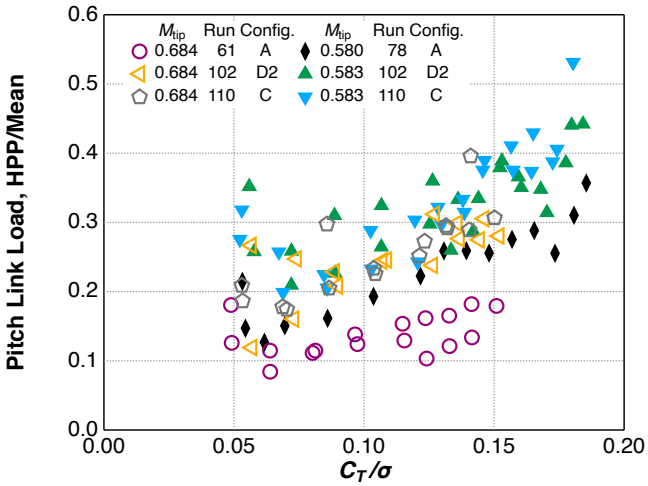

Fig. 29. TTR/699 unsteady pitch-link loads vs. thrust at two tip speeds.

REPEATABILITY

Consistency Between Runs

An important quality criterion is repeatability between runs, between tip speeds, and between increasing and decreasing thrust. Figures 26 and 27 (above) show good repeatability between tip speeds, given the same wind-tunnel configuration. Additional comparisons are shown in Figs. 30-32 for selected data. The plotted data include the best-matched data for configurations with highest thrust (Runs 60 and 61) and lowest loads (Runs 62 and 63). The figures are subsets of Figs. 9-11, replotted for ease of comparison.

Figures 30-32 also clearly reveal the effects of flow direction (yaw angle). For the selected runs, 180-deg yaw yielded higher figure of merit and airspeed, but similar climb efficiency, than 0-deg yaw. The trends are very consistent, except for climb efficiency at 180-deg yaw, which had more scatter. Closing Vane Sets 6/7 (Run 62 = closed, Run 63 = open) had little effect at 180-deg yaw (but see the earlier discussion for loads data).

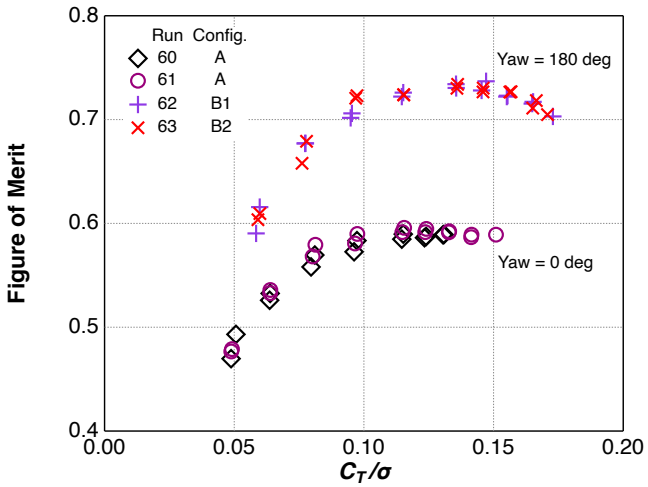

Fig. 30. Figure of merit vs. thrust at M_{tip}=0.684.

There were no repeated thrust sweeps for the JVX test, nor were there up-and-down thrust sweeps with enough data points to establish reliable trends. JVX data are therefore omitted here.

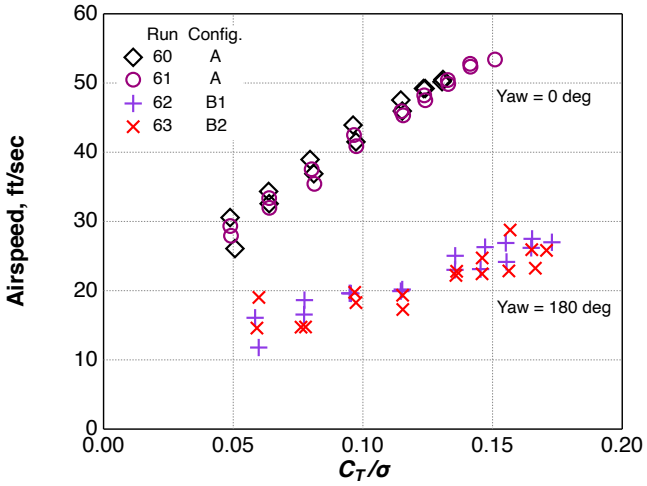

Fig. 31. Airspeed vs. thrust at M_{tip}=0.684.

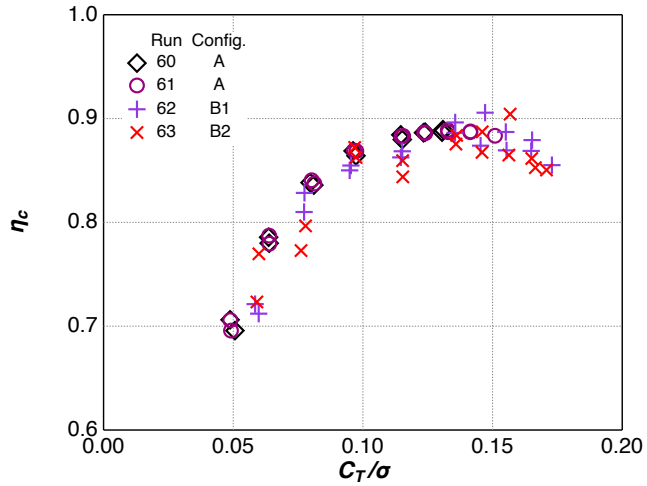

Fig. 32. Climb efficiency vs. thrust at M_{tip}=0.684.

Effects of Thrust Trend

For most TTR/699 runs, thrust was progressively increased from near-zero to maximum achievable (usually limited by hub loads), then reduced to the starting thrust. Data for ten such up/down sweeps are plotted in Figs. 33-35, including thrust sweeps at helicopter-mode and airplane-mode tip speeds (M_{tip}=0.684 and M_{tip}=0.583, respectively) in separate plots. Run 78 is omitted because a downward thrust sweep was not included in the run. Crosses denote increasing thrust, and circles denote decreasing thrust. In order to clarify the data, only four runs are shown on each figure at M_{tip}=0.684. Figure of merit is shown instead of climb efficiency because figure of merit better separates the plotted data, as appropriate for assessment of repeatability within a run (not between runs).

The rotor operator attempted to match thrust coefficient at each point during both increasing and decreasing sweeps, but in the interest of saving run time, exact matches were not pursued. Trimmed thrust is nevertheless good enough to show that repeatability of figure of merit within each run is excellent. Repeatability of airspeed is not as good, except for Runs 61 and 101.

The first and last data points of each run, at minimum thrust, did not always match each other as well as data points at higher thrust. It is possible that the mismatch occurred because the airspeed had not fully stabilized at these data points. However, the trends in figure of merit do not match those of airspeed, so this explanation remains conjectural.

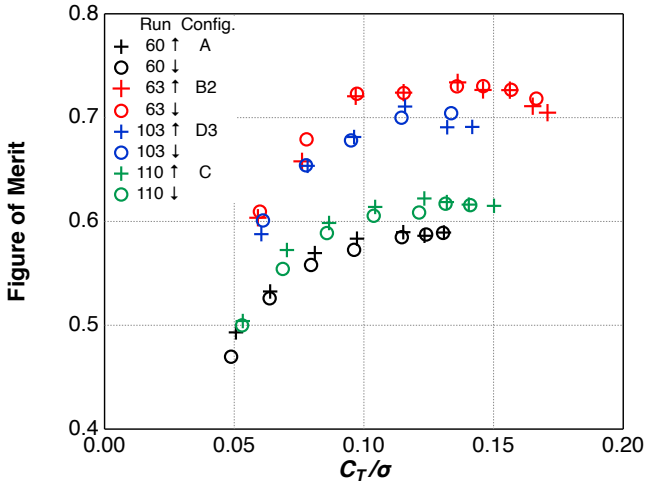

(a) Runs 60, 63, 103, and 110

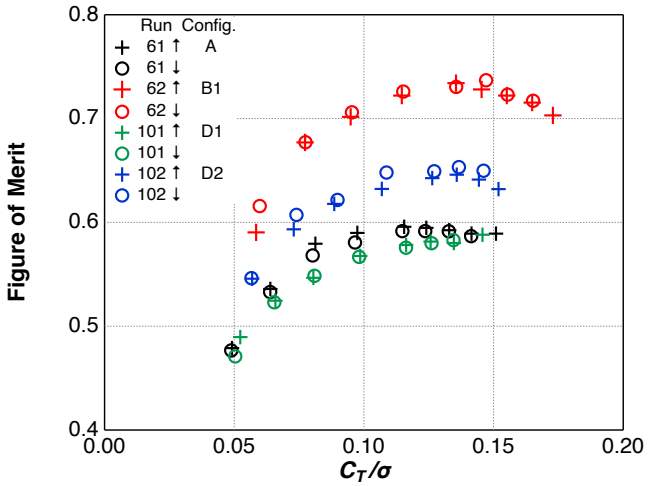

(b) Runs 61, 62, 101, and 102

Fig. 33. Figure of merit for up & down thrust sweeps at M_{tip}=0.684.

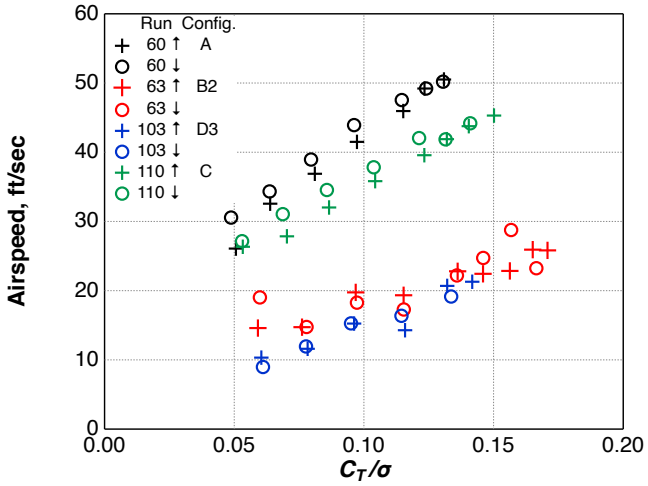

(a) Runs 60, 63, 103, and 110

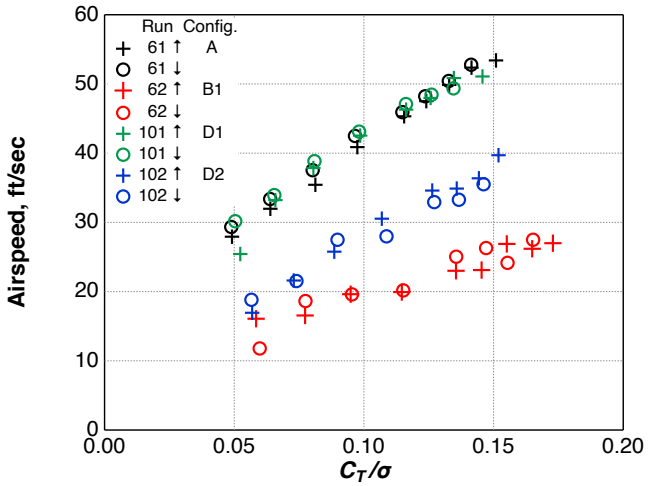

(b) Runs 61, 62, 101, and 102

Fig. 34. Airspeed for up & down thrust sweeps at M_{tip}=0.684.

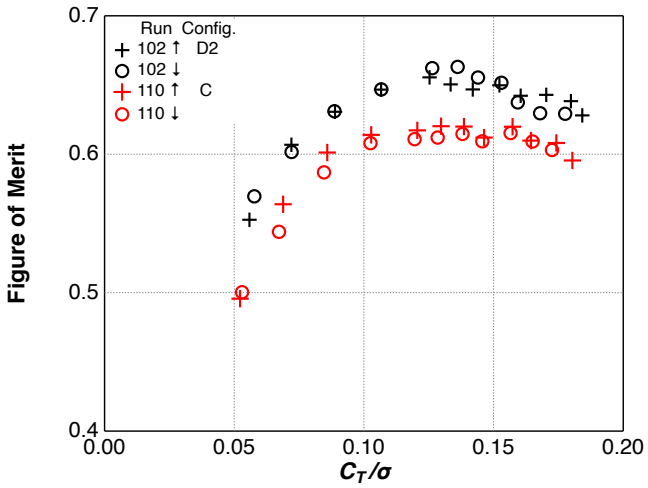

Fig. 35. Figure of merit for up & down thrust sweeps at M_{tip}=0.583.

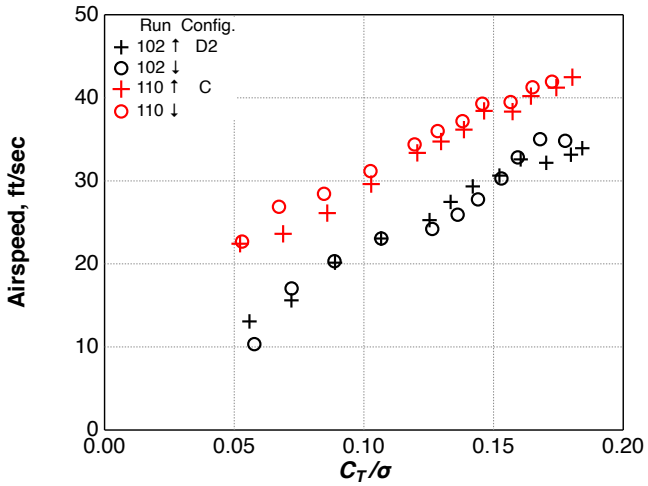

Fig. 36. Airspeed for up & down thrust sweeps at M_{tip}=0.583.

CONCLUSIONS

The TTR/699 was tested in vertical climb (near hover) conditions at a wide variety of 40x80 wind tunnel configurations, including normal upstream (0-deg yaw) and downstream (180-deg yaw) orientations. Seven different combinations of yaw angle and wind-tunnel configurations (NFAC vane set positions) were tested for the TTR/699. Test-section airspeed was that induced by the rotor. TTR/699 data were compared with the limited data available from the older PTR/JVX test (also tested in the 40x80 wind tunnel). The following conclusions can be drawn from the results presented here:

1. For the TTR/699, higher thrust at lower airspeed was achieved at 180-deg yaw than at 0-deg yaw, but at the cost of higher unsteady loads. Unsteady loads at 180-deg yaw were always higher and more sensitive to thrust (hence airspeed) than at 0-deg yaw. No configuration had lower loads than the standard 40x80 0-deg yaw configuration, but no configuration at 0-deg yaw achieved thrust as high as at 180-deg yaw. Similar results were seen at reduced tip speed.

2. The TTR/699 showed good consistency between runs, more so at 0-deg yaw than at 180-deg yaw. Comparing increasing and decreasing thrust trends within each run, consistency within each run was good, again slightly better at 0-deg yaw.

3. The PTR/JVX data showed more scatter than the TTR/699. JVX unsteady pitch-link loads varied more with thrust than 699 loads, and were almost as large as the largest 699 loads. JVX loads varied erratically with airspeed. At the same airspeed, JVX unsteady pitch-link loads were sometimes much higher than 699 loads, which indicates that steady airspeed alone cannot explain the differences. Unsteady airspeed (turbulence) was not measured and is an obvious candidate for inclusion in future research.

4. The PTR/JVX had higher measured figure of merit than the TTR/699, but with much greater scatter in climb efficiency. JVX rotor-induced airspeed was similar to the 699 at 180-deg yaw. Trimmed gimbal angle was much larger for the JVX rotor. Opening the 40x80 overhead doors decreased data quality, worsened trim, and resulted in questionable improvement in rotor performance.

Taken together, these results indicate that the hover/vertical climb PTR/JVX data should not be relied upon for research purposes, whereas the TTR/699 data are useful given the appropriate wind-tunnel configuration.

RECOMMENDATIONS

Claiming that any specific configuration yields the "best" data is unreasonable. The researcher must make a tradeoff between maximum thrust, minimum or maximum airspeed, and unsteady loads, as appropriate to the research being undertaken. Nonetheless, the standard 40x80 high-speed configuration (Configuration A) with the TTR at 0-deg yaw gives the lowest unsteady loads, and no other configuration at 0-deg yaw gives substantially higher thrust. If maximum thrust or minimum airspeed is the objective, then 180-deg yaw is appropriate, assuming increased unsteady loads are acceptable. Higher airspeeds (rate of climb) are always possible by operating the drive fans; the challenge is getting good results at low speeds.

Not all possible combinations of vane set positions and TTR orientation were tested. While minor improvements in data extent and quality could possibly be obtained with further adjustments to the wind-tunnel configuration, a more productive approach is to do near-hover testing in the larger, 80- by 120-ft test section. Testing at the OARF would be necessary to achieve true hover conditions. Given that such tests are often impractical, the smaller, 40- by 80-ft test section can provide useful data if properly interpreted.

Calibrating the NFAC air data system for reverse flow is problematic at best, and unlikely to be accurate with a rotor installed at 180-deg yaw. CFD studies have been initiated to examine the effects of reverse flow, including rotor induced velocity, on NFAC airspeed measurements.

If further testing is done at 180-deg yaw, a low-speed anemometer should be installed upstream of the rotor (downstream with respect to the test section) to measure tunnel airspeed independently of the NFAC system. Test-section wall pressure measurements would give valuable reference data for CFD studies of wall effects.

REFERENCES

1. Acree C. W., Jr., and Sheikman, A. L., "Development and Initial Testing of the Tiltrotor Test Rig," American Helicopter Society 74th Annual Forum, Phoenix, AZ, May 14-17, 2018.

2. Russell, C. R., and Acree, C. W., "Modal Test and Analysis of the NASA Tiltrotor Test Rig," American Helicopter Society Technical Conference on Aeromechanics Design for Transformative Vertical Lift, San Francisco, CA, January 16-19, 2018.

3. Acree, C. W., Jr., Sheikman, A. L., and Norman, T. R., "Wind Tunnel Performance Tests of a Full-Scale Proprotor on the Tiltrotor Test Rig," NASA TM-20210021871, December 2021.

4. Schatzman, Natasha L., and Malpica, C., "Acoustic Testing of the Tiltrotor Test Rig in the National Full-Scale Aerodynamics Complex 40- by 80-Foot Wind Tunnel," Vertical Flight Society 75th Annual Forum Proceedings, Philadelphia, PA, May 2019.

5. Kottapalli, S., and Acree, C. W., Jr., "Analytical Performance, Loads, and Aeroelastic Stability of a Full-Scale Isolated Proprotor," American Helicopter Society Technical Conference on Aeromechanics Design for Transformative Vertical Lift, San Francisco, CA, January 16-19, 2018.

6. Kottapalli, S., Russell, C. R., Acree, C. W., Jr., and Norman, T. R., "Aeroelastic Stability Analysis of a Full-Scale Isolated Proprotor on the Tiltrotor Test Rig," AIAA Paper no. 2019-2134, Dynamics Specialists Conference, AIAA SciTech Forum Proceedings, San Diego, CA, January 2019.

7. Kottapalli, S., and Acree, C. W., Jr., "Correlation of Full-Scale Isolated Proprotor Performance and Loads," Vertical Flight Society 75th Annual Forum Proceedings, Philadelphia, PA, May 2019.

8. Acree, C. W., Jr., "Vertical Climb Testing of a Full-Scale Proprotor on the Tiltrotor Test Rig," Vertical Flight Society Aeromechanics for Advanced Vertical Flight Technical Meeting, San Jose, CA, January 21–23, 2020.

9. Kottapalli, S., "Loads Correlation of a Full-Scale Proprotor on the Tiltrotor Test Rig," Vertical Flight Society Aeromechanics for Advanced Vertical Flight Technical Meeting, San Jose, CA, January 21-23, 2020.

10. Solis, E., and Meyn, L., "Photogrammetric Deflection Measurements for the Tiltrotor Test Rig (TTR) Multi-Component Rotor Balance Calibration," American Helicopter Society Technical Meeting on Aeromechanics Design for Vertical Lift Proceedings, San Francisco, CA, January 2016.

11. Felker, F. F., Signor, D. B., Young, L. A., and Betzina, M. D., "Performance and Loads Data From a Hover Test of a 0.658-Scale V-22 Rotor and Wing," NASA TM-89419, April 1987.

12. Acree, C. W., "Assessment of JVX Proprotor Performance Data in Hover and Airplane-Mode Flight Conditions," NASA/TM-2016-219070, February 2016.

13. Felker, F. F., Shinoda, P. R., Heffernan, R. M., and Sheehy, H. F., "Wing Force and Surface Pressure Data from a Hover Test of a 0.658-Scale V-22 Rotor and Wing," NASA TM-102244, February 1990.

14. Felker, F. F., "Results From a Test of a 2/3-Scale V-22 Rotor and Wing in the 40- by 80-Foot Wind Tunnel," American Helicopter Society 47th Annual Forum, Phoenix, AZ, May 1991.

15. Johnson, W., *Rotorcraft Aeromechanics*, Cambridge University Press, 2013.

16. Glauert, H., *The Elements of Aerofoil and Airscrew Theory*, Chap. XVII, pp. 222–226, Cambridge University Press, 2nd Ed., 1947.